*fractal and fractional*

MDPI

*Article*

# Fractional Order Weighted Mixed Sensitivity-Based Robust Controller Design and Application for a Nonlinear System

**Erdem Ilten**

Department of Electrical-Electronics Engineering, Balikesir University, Balikesir 10145, Turkey; erdemilten@balikesir.edu.tr

**Abstract:** This paper focuses on fractional-order modeling and the design of a robust speed controller for a nonlinear system. An induction motor (IM), widely used in Electrical Vehicles (EVs), is preferred in this study as a well-known nonlinear system. The major challenge in designing a robust speed controller for IM is the insufficiency of the machine model due to inherent machine dynamics. Fractional calculus is employed to model the IM using the small-signal method, accounting for model uncertainties. In this context, experimental data is approximated using a fractional-order small-signal transfer function. Consequently, a mixed sensitivity problem is formulated with fractional-order weighting functions. The primary advantage of these weighting functions is their greater flexibility in solving the mixed sensitivity problem by involving more coefficients. Hereby, three robust speed controllers are designed using the PID toolkit of the Matlab program and solving the $H_\infty$ mixed sensitivity problem, respectively. The novelty and contribution of the proposed method lie in maintaining the closed-loop response within a secure margin determined by fractional weighting functions while addressing the controller design. After evaluating the robust speed controllers with Bode diagrams, it is proven that all the designed controllers meet the desired nominal performance and robustness criteria. Subsequently, real-time implementations of the designed controllers are performed using the dsPIC microcontroller unit. Experimental results confirm that the designed $H_\infty$-based fractional-order proportional-integral-derivative (FOPID) controller performs well in terms of tracking dynamics, exhibits robustness against load disturbances, and effectively suppresses sensor noise compared to the robust PID and fixed-structured $H_\infty$ controller.

**Keywords:** fractional calculus; weighted-mixed sensitivity; robust control; small-signal model; induction motor



**Citation:** Ilten, E. Fractional Order Weighted Mixed Sensitivity-Based Robust Controller Design and Application for a Nonlinear System. *Fractal Fract.* **2023**, *7*, 769. https://doi.org/10.3390/fractalfract7100769

Academic Editors: Miguel A. Platas-Garza, Cornelio Posadas-Castillo and Ernesto Zambrano-Serrano

Received: 29 August 2023
Revised: 13 October 2023
Accepted: 18 October 2023
Published: 19 October 2023



## 1. Introduction

### 1.1. The Contex of Research

The irrational exploitation of existing fossil resources leads to environmental pollution and adversely affects the health of all living beings. Consequently, the depletion of fossil resources and growing environmental concerns have driven researchers and decision-makers to adopt EVs. Among the various drive systems used in EVs, the induction motor system stands out as a highly employed option. It has demonstrated its attractiveness in comparison to direct current (DC) motor systems due to several reasons, including cost-effectiveness, robust structure, and lower maintenance requirements [1]. However, ensuring the robustness of the speed control scheme is essential. This necessitates the design of an appropriate system model and a suitable speed controller [2]. Addressing these challenges constitutes the primary focus of most researchers engaged in the study of induction motors for EV applications.

### 1.2. Literature Review

Recent times have witnessed a surge in modeling and the design of robust controllers for induction motor (IM) systems, sparking a multitude of studies within the control

community. Talla et al. proposed an adaptive speed controller for IM that leveraged imprecise models containing compensators to address nonlinearity and uncertainty. Their approach's robustness was validated through the Lyapunov theorem [3]. Sung et al. prioritized energy efficiency through the adoption of maximum torque per ampere control, bolstered by compensatory measures for flux, temperature, and voltage variations, ensuring robustness [4]. Lin and Wai explored a neural network-based uncertainty observer as an integral part of a robust IM controller [5]. Alonge et al. introduced two linear extended state observers for IM to counter both internal and external disturbances, incorporating a sliding mode-based component to achieve complete robustness [6]. Pohl and Vesely applied the $H_\infty$ technique to IM speed control, utilizing the d-q equivalent circuit of the IM for controller design [7]. Qu and Zhao addressed denial-of-service attacks through an acknowledgment mechanism, devising an $H_\infty$ controller for type-2 fuzzy systems under such attacks [8]. Given these aforementioned studies, it is evident that designing a speed controller for IM is no straightforward task. Despite the manifold advantages of IMs, their control systems remain intricate. Nevertheless, scalar control techniques offer a straightforward algorithm and enhanced performance in steady states [9].

$H_\infty$ control, employed alongside scalar control methods, offers a promising approach to mitigate the intricacies inherent in the IM speed control system. Its capacity for robust stability and meeting nominal performance conditions is encapsulated within a weighted-mixed sensitivity problem formulation. Within the $H_\infty$ framework, a robust controller can be ascertained. A multitude of researchers have harnessed $H_\infty$-based robust control techniques to govern the speed of IMs. Acevedo et al. utilized $H_\infty$ control in tandem with a loop shaping procedure to govern both dynamic and steady-state responses of IMs. They achieved linearity in the rotor flux-oriented model via Taylor's series [10]. Mohamed, considering model uncertainties and the suboptimal performance of IMs, proposed an $H_\infty$ loop shaping design procedure to formulate a speed controller. He represented nonlinear dynamic equations in state-space form and synthesized a robust controller by selecting frequency shaping functions. The results highlighted an acceptable trade-off between robust stability and performance [11]. Allag et al. introduced robust H∞ control for the field-oriented control of IMs. They transformed the nonlinear IM model into the Takagi-Sugeno form and determined controller gains by solving linear matrix inequalities [12]. Among the range of methods for synthesizing $H_\infty$ controllers, many scholars have gravitated toward the automatic selection of weighted-mixed sensitivity problems. This approach relies on well-chosen performance and stability weights, resulting in robust control and superior tracking performance when dealing with well-modeled systems and parameter values confined within specified bounds. Consequently, fixed integer weights have found widespread application in robust controller designs across various industrial sectors. Kaitwanidvilai et al. presented a Particle Swarm Optimization (PSO)-based approach for automatically selecting weights in an interconnected power system. The effectiveness of the method was verified, showing enhanced stability margins for the designed controller [13]. Kaur and Ohri showcased the application of PSO-based tuning for weighting functions, resulting in improved tracking performance. The automatic selection method demonstrated robustness against plant perturbations and disturbances [14].

On the other hand, the robustness margin of $H_\infty$ controllers can be further expanded through the incorporation of fractional-order Laplace operators. This approach introduces more adaptable weighting functions with a variety of adjustable parameters for mixed sensitivity problems, thereby offering increased flexibility [15]. Fractional-order Laplace operators are a term of fractional calculus which has gained substantial popularity within the control community [16–21]. In this context, this operator has been used in $H_\infty$ controllers, either in design step or in controller structure. Sedraoui et al. implemented adjustable fractional weights within the mixed sensitivity weighting problem, aiming to enhance both nominal performance and robust stability margins for an induction generator [22]. Notably, they employed an extracted continuous-time linear state space model centered around an operational point, utilizing the Matlab/Simulink program. Amieur et al. sought to enhance

the trade-off between nominal performance and robust stability within closed-loop systems. Their approach involved the utilization of a min-max optimization algorithm to fine-tune the robust controller [23]. While Reference [22] employs controllers with integer orders, Reference [23] utilizes controllers with fractional orders and fractional weights in the $H_\infty$ method. Menak and Tan introduced a novel fitness function that combines constraints related to $H_\infty$ robust performance and Bode's ideal transfer function. They employed the PSO algorithm to minimize this fitness function, effectively tuning the parameters of the FOPID controller [24]. Yaghi and Efe presented a method for enhancing the stability and tracking performance of the FOPID controller, combining a neural tuning technique with $H_2/H_\infty$ optimization [25]. Majid et al. put forth an innovative approach for designing an $H_\infty$-optimal FOPID controller capable of managing transient, steady-state responses, and stability margins. They applied this method to a phase-locked-loop motor speed system and an electromagnetic suspension system, providing examples that demonstrate the design process and validate the performance of the proposed controller. The results indicate that the proposed approach enhances system responses compared to the traditional $H_\infty$-optimal controller while still preserving $H_\infty$ optimality [26]. References [24–26] adopt fractional-order controllers with integer-order weights within the $H_\infty$ method.

### *1.3. Research Gaps*

It is worth noting that, especially within IM speed control schemes, there has been a lack of experimental exploration into the application of fractional operators within $H_\infty$ control design methodologies. Brief literature review shows that fractional-order weighting functions have not been implemented experimentally in mixed sensitivity problems for a nonlinear system. Moreover, all the designed robust controllers are viable when the model of the system (IM in this study) or its dynamic equations are already known. However, in many industrial implementations, an accurate model is often lacking due to the presence of inherent system dynamics, such as unexpected nonlinear behaviors or unmodeled dynamics. This situation is particularly pronounced in the drive systems of IMs, leading to a scarcity of sufficient mathematical models. Furthermore, the complexity of designing a speed controller is increased without an adequate machine model.

Compared to previous studies, the application of fractional-order modeling and the design of a robust controller based on fractional-order weights within the mixed sensitivity problem for IM systems has not been attempted before. However, the lack of prior knowledge concerning the inherent dynamics of IM and the unknown parameters of the equivalent circuit present significant challenges. When these challenges are compounded by the limitations of the dsPIC microcontroller's performance during real-time implementation, the stages of modeling and controller design become considerably more intricate.

### *1.4. Authors' Contribution*

In this study, we propose a closed-loop modeling approach for the actual IM behavior based on the fractional-order small signal method to address model uncertainties. A primary advantage of small signal modeling lies in its simplicity while maintaining accuracy [27]. Notably, the utilization of more adaptable fractional-order small signal models based on non-integer order Laplace operators can enable precise design. This technique offers a linear model for the speed control scheme, encompassing the nonlinear IM behavior around its operational point. The modeling step employs the FOMCON toolbox, a Matlab software (R2022a) designed by Tepljakov [28]. It is crucial that the overall state of the IM system remains stable after the transient response during the modeling process. Essentially, small perturbations can be introduced to diversify the input-output dataset. As a result, this technique finds widespread application in the modeling of nonlinear systems. Subsequently, the study focuses on the design of a robust controller based on fractional-order weights within the mixed sensitivity problem for IM systems. Based on these explanations, the main contributions can be highlighted as follows:

- Fractional-order small signal modeling for IM is undertaken for the first time, achieved through the approximation of experimental data.
- The fractional Laplace operator is incorporated in weighting functions, following to the general guidelines of mixed sensitivity.
- Optimal parameters are determined to enhance the robust stability and nominal performance of the closed-loop system with the designed controller.
- Three distinct robust controllers (Robust PID Controller, FOPID Based $H_\infty$ Controller and Fixed-structure $H_\infty$ controller) are designed and compared in terms of robustness and tracking performances.

The design of robust controllers and weighting functions is indeed carried out concurrently. PSO is employed to determine the parameters of the weighting functions, in conjunction with the fractional Laplace operator, as well as the controller parameters. Initially, a robust PID controller is formulated using the Matlab software toolbox. Subsequently, utilizing the robust control toolbox within Matlab, a structured reduced-order H∞ controller is designed. The rationale for reducing the order of this controller is based on the performance limitations of the dSPIC microcontroller board. Finally, a FOPID controller is synthesized by solving the weighted mixed sensitivity problem. Experimental tests are executed under conditions of load disturbances and sensor noises to validate whether the proposed controllers meet the specified criteria for nominal performance and robust stability margins. Hence, the novelty of this paper lies in the integration of fractional order small signal modeling with fractional order weights, which are used in the synthesis of a robust speed controller.

### *1.5. Chapter Organization*

This paper is organized into five sections. Section 2 provides a brief description of the IM system, including mathematical expressions, the experimental setup, and fractional-order small signal modeling. In Section 3, detailed explanations of the $H_\infty$ mixed sensitivity method and the design of robust controllers are presented. The design subsections also include in-dept analysis and comparisons. Section 4 encompasses the experimental studies along with results and discussions. Finally, Section 5 serves as the conclusion.

## 2. Modeling of Induction Motor System

For rotor flux $\lambda$ (Wb), α-β axis stator current (A) equations of an induction motor [29] can be written as follows:

$$\frac{di_\alpha}{dt} = k_1\left(\eta\lambda_\alpha + \omega\lambda_\beta\right) - k_2 i_\alpha + k_3 u_\alpha \tag{1}$$

$$\frac{di_\beta}{dt} = k_1\left(\eta\lambda_\beta + \omega\lambda_\alpha\right) - k_2 i_\beta + k_3 u_\beta \tag{2}$$

In Equations (1) and (2), $k_1 = \frac{L_m}{\sigma L_s L_r}$, $k_2 = \frac{R_s L_r^2 + R_r L_m^2}{\sigma L_s L_r^2}$, $k_3 = \frac{1}{\sigma L_s}$, $\sigma = 1 - \frac{L_m^2}{L_s L_r}$, $\eta = \frac{R_r}{L_r}$, $u_\alpha$ (V) and $u_\beta$ (V) are stator voltages, $R_s$ (Ω) and $R_r$ (Ω) are resistances of the stator and rotor, $L_s$ (H) and $L_r$ (H) are inductances of stator and rotor. $L_m$ (H) denotes the mutual inductance and $\omega$ (rad/s) represents the angular speed. α-β axis rotor flux equations are defined as below:

$$\frac{d\lambda_\alpha}{dt} = -\eta\lambda_\alpha - \omega\lambda_\beta + \eta L_m i_\alpha \tag{3}$$

$$\frac{d\lambda_\beta}{dt} = -\eta\lambda_\beta - \omega\lambda_\alpha + \eta L_m i_\beta \tag{4}$$

Equation of angular speed $\omega_r$ is given as follows:

$$\frac{d\omega_r}{dt} = \frac{p}{J}\frac{L_m}{L_r}\left(\lambda_\alpha i_\beta - \lambda_\beta i_\alpha\right) - \frac{B}{J}\omega - \frac{1}{J}T_L \tag{5}$$

$B$ (N·m·s) is friction factor, $J$ (kg·m$^2$) is rotor inertia, $T_L$ (Nm) is load torque and $p$ is pole pairs in Equation (5). Block diagram of IM system is represented in Figure 1. In this scheme, IM angular speed is measured with an encoder and motor is loaded with electromagnetic brake. IM is powered by a 3-phase inverter and the brake is supplied wtih DC power supply. The measurement of IM's angular speed, the operation of the speed control algorithm, the switching of the load and/or noise on/off, and the data transfer to the PC are all achieved with a digital signal processor (DSP).

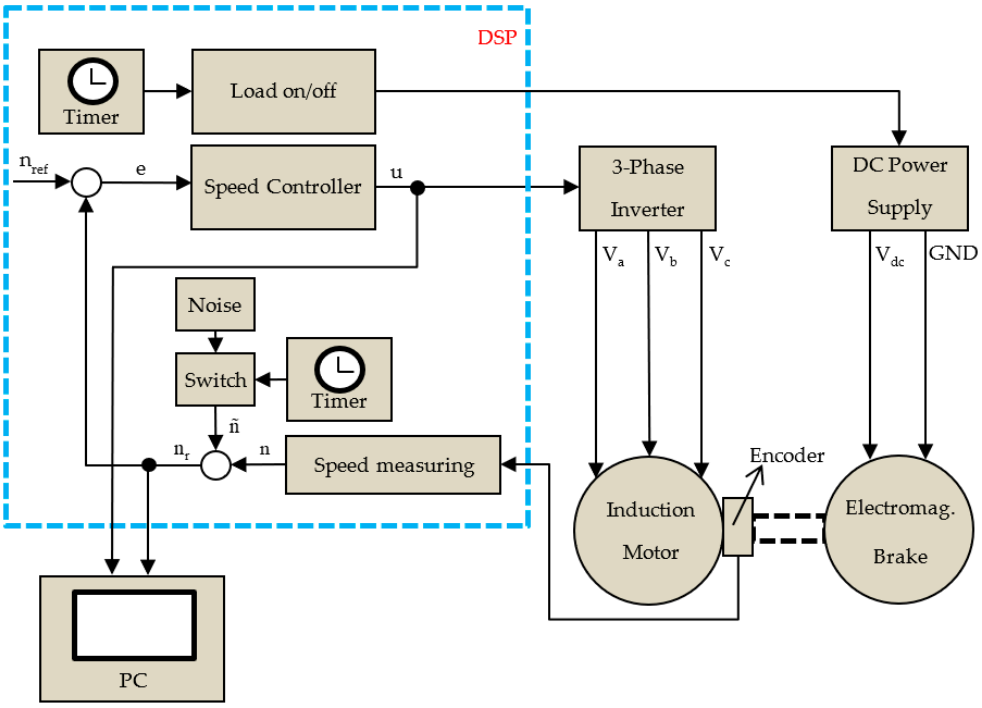


**Figure 1.** Block diagram of IM system.

In Figure 1, $u$ represents the speed controller output signal, n is the actual speed, $\tilde{n}$ is the artificial measurement noise, $n_r$ is the measured speed with noise, $n_{ref}$ denotes the reference speed, $e$ is the speed error between $n_{ref}$ and $n$. $u$ and $n$ data are stored on the PC for generating system and controller models. The original part in block diagram is the method used in the speed controller block. Artificial noise is introduced to the system for a specific duration to assess the controllers' performance against sensor noise.

### *2.1. Description of Experimental Setup*

The IM speed control system is designed to test various controller methods and to compare their performance. In the experimental studies, dsPIC33FJ128MC804 microcontroller serves as the DSP unit to measure the motor speed from the encoder and operate the speed control methods. Furthermore, the actual motor speed and controller output signal are transmitted to the PC for data logging and monitoring. The experimental setup is depicted in Figure 2.

In Figure 2, the setup comprises a 3-phase induction motor, an electromagnetic brake, an optical 1024 pulses per revolution (PPR) encoder, a 3-phase 3 kW inverter, a regulated DC power supply with an output of 0–30 V 6 A, controller cards (dsPIC, PIC programmer, UART-USB converter, 5 V DC power supply, 3.3 V DC power supply) and a PC. The machine parameters of the IM are listed in Table 1.

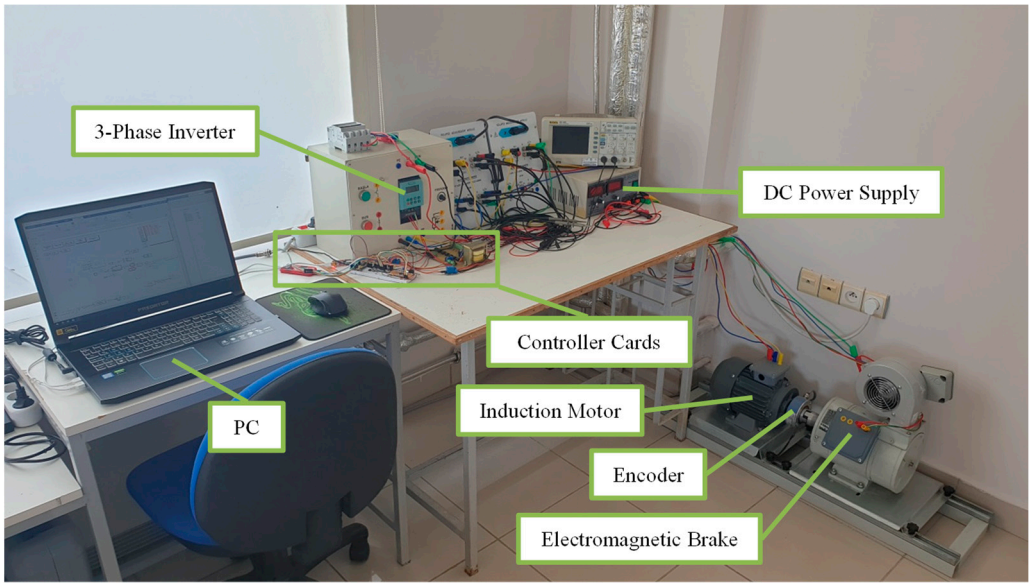


**Figure 2.** Experimental setup.

**Table 1.** IM parameters.

| Parameter | Value |
|---|---|
| Rated Voltage ($V_{L\text{-}N}$) | 220 V |
| Rated Current | 2.7 A |
| Rated Power | 1.1 kW |
| Frequency | 50 Hz |
| Cosine ($\varphi$) | 0.80 |
| Rated Speed | 1380 rpm |
| Pole pairs ($p$) | 2 |
| Stator Resistance ($R_s$) | 7.8 Ω |
| Stator Inductance ($L_s$) | 55 mH |
| Friction Factor ($B$) | 0.072 N·m·s |
| Rotor Inertia ($J$) | 0.0088 kg·m$^2$ |

### *2.2. Fractional Order Small Signal Modeling of IM*

This paper employs the small signal transfer function of an IM to facilitate frequency domain control design. The transfer function is derived from the small signal model, which linearizes the actual behavior of the IM around its operational point. Drawing on insights from previously published papers, small signal modeling has the advantage of mitigating the impact of unmodeled dynamics and nonlinear behaviors [27,30]. Consequently, the modeling step does not necessitate the inclusion of all equivalent circuit parameters or intricate details of the IM. As a result, the process of implementing small signal modeling comprises three steps: constructing the large signals of the input-output measurement dataset, processing the large signal by subtracting average values, and deriving the small-signal transfer function for the angular speed of the induction motor. In a departure from studies in existing literature, this research not only focuses on devising a convenient small signal model for the induction motor but also incorporates the fractional Laplace operator to achieve a more flexible model. The innovation presented here lies in the determination of an accurate fractional order small signal model, offering greater flexibility for user-adjustable coefficients. This approach allows for the capture of a more sensitive transfer function while disregarding numerous unmodeled dynamics.

This section focuses on the design of a fractional-order small signal model for the IM using the measured input-output dataset. As explained in the description of the experimental setup, the IM control system is driven by a pulse width modulation signal (PWM) with a 0–100% duty cycle. Simultaneously, the speed response is monitored by

an encoder, producing values ranging from 0 to 1500 rpm. During the modeling phase, the system is subject to random triggering, and the outcomes are documented as shown in Figure 3a and Figure 3b, respectively. This process results in the creation of a large signal input-output dataset. Subsequently, calculations reveal that the mean values of the triggering command and speed are 73.6% and 988.779 rpm, respectively. Using the average variable method, these mean values are extracted from the large signals, leading to the generation of the processed triggering command ($u$) and measured speed ($n$), as illustrated in Figure 3c and Figure 3d, respectively.

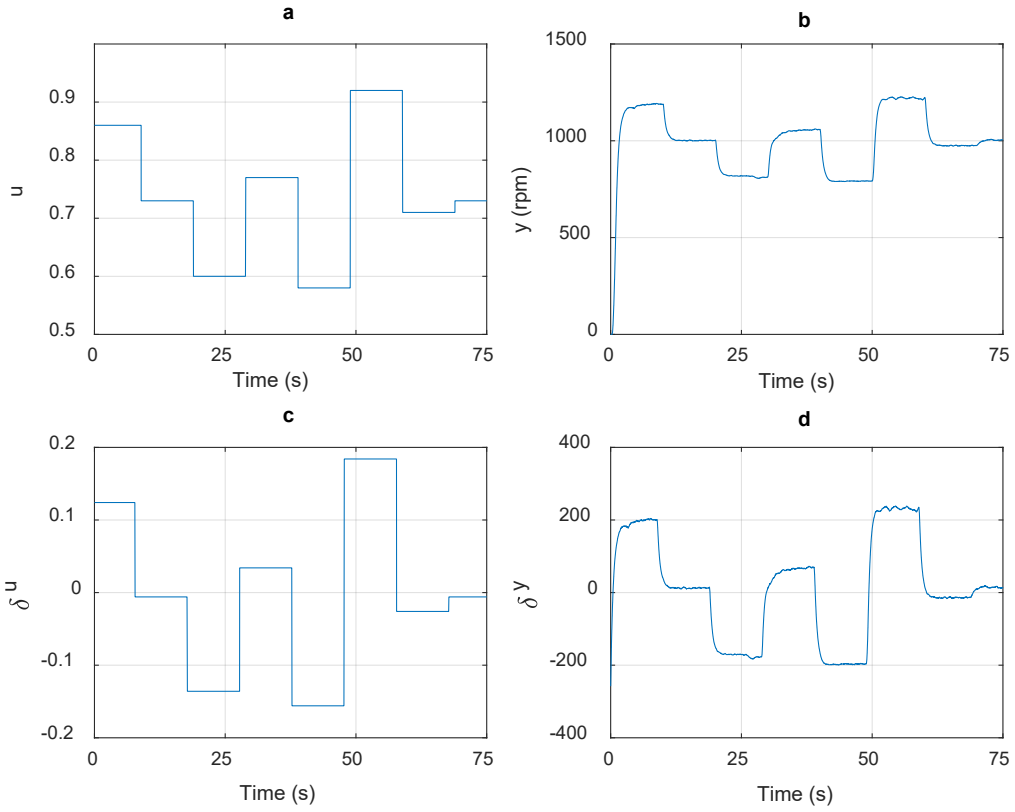


**Figure 3.** Measured and processed data set used for modeling. (**a**) random triggering input, (**b**) speed output, (**c**) small-signal input, (**d**) small-signal output.

The δu and δy values in Figure 3c,d are small-signal input and output values, respectively. The primary objective is to design the intended fractional-order small-signal model using the FOMCON toolbox within the Matlab software (R2022a) [28]. In the case of a black-box model, an input-output dataset is required, and the model output error is minimized through the least squares approach. Fractional calculus serves as a generalization of traditional calculus. Thus, to achieve a more precise representation of the system dynamics, the Grünwald–Letnikov definition-based numeric solver is adopted, eschewing classical differential equations. The identification problem is formulated as an estimation of a set of parameters, including zeros, poles, and coefficients.

Based on preliminary investigations, it has been determined that the system is characterized by six poles and two zeros, a specification incorporated into the toolbox. Notably, a trial-and-error approach is utilized to identify the optimal zero-pole combination. To perform the nonlinear least-squares estimation of model parameters, the Levenberg–Marquardt algorithm is employed. Subsequently, applying the 'fid' command yields the desired fractional-order small-signal model for speed, achieving an impressive 95.69% model accuracy. The resultant transfer function is expressed as Equation (6).

$$G_s = \frac{1e^{-5}s^{1.9980} + 9300.2s^{\,0.9769} + 0.1606}{0.0073s^{5.9567} + 2.2133s^{4.0961} + 10s^{3.0156} + 6.2218s^{2.0473} + 5.3874s^{1.5051} + 5.4717s^{\,0.9998} + 1e^{-5}} \quad (6)$$

In continuous-time systems, stability is indicated when all poles are located in the open left half of the complex plane. The 'isstable($G_s$)' function in Matlab provides a logical value of 1 (true) as an indicator of dynamic system stability. However, the transfer function designed here incorporates fractional-order Laplace operators. To use the 'isstable' function in this context, we employ an approximate transfer function obtained using the 'fid' function. The resulting value of 1 serves as confirmation of the stability of $G_s$'s. Figure 4 displays the validation of the designed small-signal model where the red line is the actual speed of IM and the blue line is the model output. The δn value in Figure 4 is the small-signal speed value. It is evident from the figure that the obtained fractional-order small signal model is capable of matching the actual behavior of the IM. This demonstrates that the designed model can be effectively used in the controller design step.

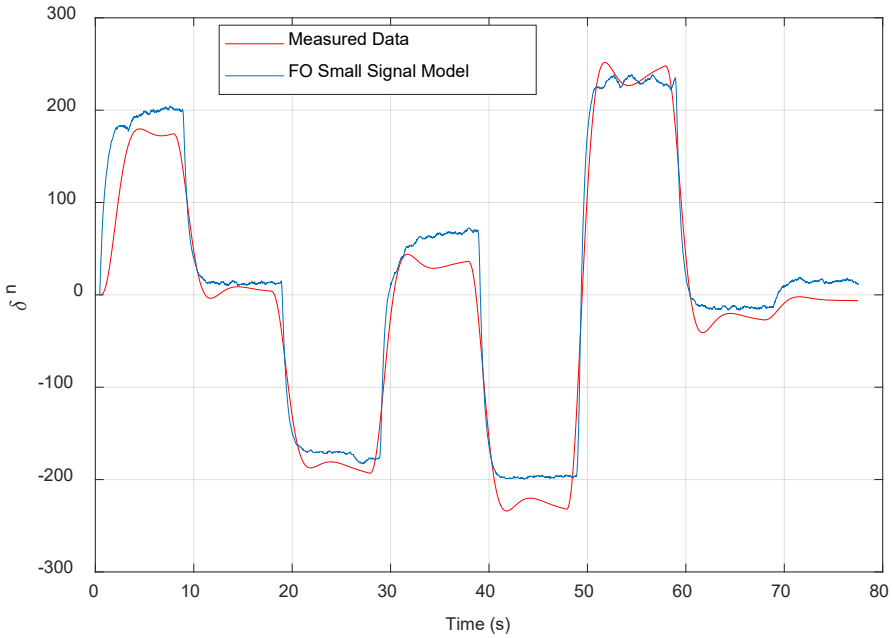


**Figure 4.** Validation of the determined fractional order small signal model.

## 3. Weighting Mixed-Sensitivity-Based $H_\infty$ Controller Design

The primary advantage of $H_\infty$ control is its capability to manage both model uncertainties and external disturbances simultaneously. In the standard $H_\infty$ control problem, as illustrated in Figure 5, external disturbance, measurable output and control signal are defined as $d$, $y$ and $u$, respectively. The robust controller $K(s)$ is designed to stabilize the closed-loop plant $P$ and minimize the norm from $d$ to $z$ at any frequency.

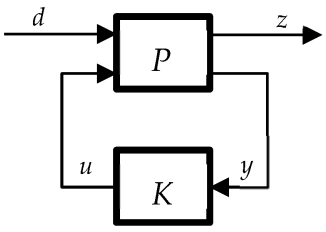


**Figure 5.** Generalized plant.

Weighted mixed-based $H_\infty$ control is a specific case of the standard $H_\infty$ optimization problem. In this study, the weighted mixed sensitivity problem is tackled to design the optimal control system that ensures the desired performance criteria by adjusting the various sensitivity functions. Thus, the performance requirements for the closed-loop system are transformed into a $H_\infty$ optimization framework with the aid of weighting functions. Based on the selected weights and performance criteria, three distinct robust controllers are designed in this section.

### *3.1. Main Concepts of $H_\infty$ Control Based on Weighted Mixed Sensitivity*

In the process of designing a robust $H_\infty$ controller, a weighted mixed sensitivity-based approach primarily focuses on the combination of disturbance attenuation with stability margin specifications [31]. Along with other criteria, the controller design problem is formulated based on three sensitivity functions: sensitivity ($S$), control sensitivity ($KS$) and complementary sensitivity ($T$). The sensitivity functions are determined as follows:

$$\begin{aligned} S &= (1 + GK)^{-1} \\ KS &= K(I + GK)^{-1} \\ T &= GK(I + GK)^{-1} \end{aligned} \tag{7}$$

Here, $G$ represents the transfer function of $P$ and $K$ is the transfer function of the robust controller. During the controller design step, the following specifications are considered: good disturbance rejection is ensured by keeping the $\|S\|_\infty$ minimum at low frequencies; effective rejection of sensor noise is achieved by minimizing the $\|T\|_\infty$ at high frequencies; and good tracking dynamics are obtained by maintaining $\|T\|_\infty$ as unity [32]. Based on these sensitivity functions and a given plant $P$, a single infinity norm function is determined as follows:

$$P = \left\| \begin{matrix} W_s S \\ W_{ks} KS \\ W_t T \end{matrix} \right\|_\infty \tag{8}$$

Here, $W_s$, $W_{ks}$ and $W_t$ are considered as the three weighting functions used in the design of $K$. Hereby, the design of the $H_\infty$ controller can be represented as an augmented plant model with respect to the given weighting functions as depicted in Figure 6. Proper selection of $W_s$, $W_{ks}$ and $W_t$ is essential to meet the specified performance requirements. Good disturbance rejection can be ensured by choosing $W_s$ within desired control bandwidth. Control effort is limited by adjusting $W_{ks}$ to prevent oscillations and sudden fluctuations in the control signal. $W_t$ is generally chosen as a high-pass filter to suppress model uncertainties or sensor noises.

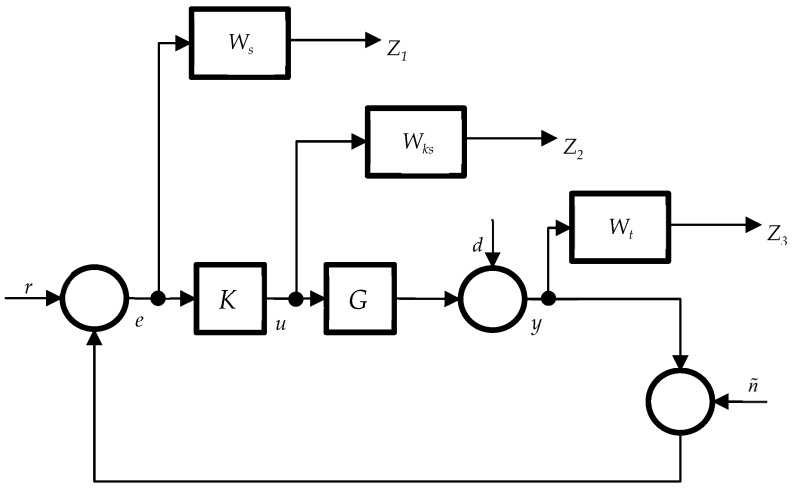


**Figure 6.** Weighted mixed sensitivity problem.

The infinity norm function (Equation (8)) is minimized to design the mixed sensitivity problem-based controller ($K$). Consequently, a performance criterion, denoted as $\gamma$, is established to maintain the infinity norm below a specific threshold. This transformation results in Equation (9), which achieves a balance between nominal performance and robust stability.

$$\left\| \begin{matrix} W_s S \\ W_{ks} KS \\ W_t T \end{matrix} \right\|_\infty \leq \gamma < 1 \tag{9}$$

The desired controller must satisfy all the specified conditions outlined in Equation (9). Therefore, the singular value plots of conditions ($\overline{\sigma}(W_s S), \overline{\sigma}(W_{ks} KS), \overline{\sigma}(W_t T)$) are considered as thresholds, and the desired controller must attenuate the worst case of these thresholds within the predetermined frequency range. This process transforms the previous $H_\infty$ optimal control problem into a suboptimal min-max problem, as follows:

$$Min \left\{ Max \left( \overline{\sigma} \left( \begin{matrix} W_s S \\ W_{ks} KS \\ W_t T \end{matrix} \right) \right) \right\} \tag{10}$$

### *3.2. Fractional Order Weighted Mixed Sensitivity Problem*

It is important to note that the weights play a significant role in the mixed sensitivity problem. The closed-loop transfer functions $S$, $R$ and $T$ are influenced by weight adjustments. As there are no specific rules to follow, certain criteria must be employed to ensure an appropriate synthesis of the $H_\infty$ controller. $W_s$ and $W_t$ are related to the magnitude of transfer functions $S$ and $T$, respectively. Their determination is provided in Equation (11) [33]

$$\begin{aligned} W_s(s) &= \frac{\left( \frac{s}{M_p^{1/n}} + \omega_{BP} \right)}{\left( s + \omega_B A_S^{1/n} \right)^n} \\ W_T(s) &= \frac{\left( s M_T^{1/n} + \omega_{BT} \right)^n}{\left( s A_T^{1/n} + M_T \omega_{BT} \right)^n} \end{aligned} \tag{11}$$

where $M_p$ and $M_T$ are the upper bounds of $S$ and $T$ within the bandwidth $\omega_{BP}$ and $\omega_{BT}$, respectively. $A_s$ is the lower limit of $S$ at low frequencies, while $A_T$ is the upper limit of $T$ at high frequencies. The variable $n$ represents the order of weights and is set to '1' in this study. By choosing appropriate gains, $W_s$ exhibits low-pass characteristics, guaranteeing good tracking dynamics with disturbance rejection. $W_t$ possesses high-pass characteristics and ensures robust stability against all possible uncertainties. Additionally, $W_{KS}$ can be chosen as a first or second-order low-pass filter to penalize the control signal. Based on Equations (9) and (10), both $W_S^{-1}$ and $W_T^{-1}$ must meet the following conditions in all frequency domains.

$$\begin{aligned} \overline{\sigma}[S] &< \overline{\sigma} \left[ W_S^{-1} \right] \\ \overline{\sigma}[T] &< \overline{\sigma} \left[ W_T^{-1} \right] \end{aligned} \tag{12}$$

General guidelines for weights selection can be explained as follows [34]:

1. It is recommended to have $A_s \ll M_P$ and $A_T \ll M_T$ to ensure that the frequency responses of weighting functions are maximally flat in the high and low frequency ranges.
2. High-performance tracking dynamics with acceptable noise levels are achieved with $\omega_{BP} < \omega_{BT}$.
3. Effective disturbance attenuation is achieved by increasing $\omega_{BP}$ as much as possible until it no longer causes a peak in the sensitivity curve.
4. When considering measurement noise, it becomes necessary to decrease $\omega_{BT}$ until it starts affecting tracking performance.

In this study, a fractional Laplace operator is utilized in weighting functions (Equation (11)) to enhance the trade-off between robust stability and nominal performance [22]. Thus, the goal is to improve controller performance in cases of load disturbance and sensor noises, regardless of restrictions in tracking dynamics. By substituting the fractional Laplace operator into Equation (11), the following fractional weighting functions are derived.

$$\begin{aligned} W_{fs}(s) &= \frac{\left(\frac{s^{\lambda_1}}{M_p^{1/n}}+\omega_{BP}\right)}{\left(s^{\lambda_1}+\omega_B A_S^{1/n}\right)^n} \\ W_{fT}(s) &= \frac{\left(s^{\lambda_2} M_T^{1/n}+\omega_{BT}\right)^n}{\left(s^{\lambda_2} A_T^{1/n}+M_T\omega_{BT}\right)^n} \end{aligned} \tag{13}$$

Here, $\lambda_{1,2}$ denotes the order of the Laplace operator, and it is chosen within the range of $0 < \lambda_{1,2} < 1$. It is evident that the robustness and performance of the designed controllers are adjusted by accurately determining the order of the weightings. Given the frequency response constraints of the sensitivity functions, the selection of appropriate weighting functions becomes more crucial during the stage of designing robust controllers.

### *3.3. Selecting of Weighting Functions*

In the controller design step, the proposed fractional weights, as given in Equation (13), are substituted in Equation (10), transforming the min-max optimization problem into Equation (14).

$$Min\left\{ Max\left(\overline{\sigma}\begin{pmatrix} W_{fs}S \\ W_{ft}T \end{pmatrix}\right)\right\} \tag{14}$$

Consequently, the design parameters vector can be defined as $dp = [M_p, \lambda_1, \omega_{BP}, M_T, \lambda_2, \omega_{BT}]$. According to the detailed guidelines provided in [34], $M_p$ and $M_T$ represent the desired minimum $H_\infty$ peak values that fulfill the conditions $\|S\|_\infty \leq M_p$ and $\|T\|_\infty \leq M_T$, respectively. Additionally, the bandwidth $\omega_{BP}$ is chosen to be larger than the crossover frequency of the system ($\omega_{BP} < \omega_c$). The desired tracking error can be adjusted by defining $A_s$. On the other hand, the desired steady state error can be kept in a bandwidth by specifying $A_T$ [27]. So, decreasing $M_p$ as much as possible enhances nominal performance ($W_sS$), however, it may violate robust stability ($W_tT$). On the contrary, minimizing $M_T$ as much as possible improves robust stability until it violates nominal performance. Therefore, upper and lower bounds of both parameters need to be determined through preliminary experiments. Since the control aim is to suppress measurement noises, $\omega_{BT}$ should be assigned meticulously. Moreover, to improve the nominal performance, $\omega_{BP}$ should be defined precisely. Hence, constrains of the *dp* are kept within the range as given in Equation (15).

$$\begin{gathered} M_{P\_\min} < M_P < M_{P\_\max} \\ \lambda_{1\_\min} < \lambda_1 < \lambda_{1\_\max} \\ \omega_{BP\_\min} < \omega_{BP} < \omega_{BP\_\max} \\ M_{T\_\min} < M_T < M_{T\_\max} \\ \lambda_{2\_\min} < \lambda_2 < \lambda_{2\_\max} \\ \omega_{BT\_\min} < \omega_{BT} < \omega_{BT\_\max} \end{gathered} \tag{15}$$

### *3.4. Design of Proposed Robust Controllers*

Two distinct $H_\infty$ controllers based on fractional order weighting functions are developed in this study. Furthermore, for the purpose of comparison, a robust PID controller is synthesized using the Matlab function *pidtool*. The control framework includes the measurement of rotor speed and the generation of triggering commands, utilizing small signals and average values to produce the actual control signal. The fractional-order small-signal-based control scheme is illustrated in Figure 7. Considering the limited performance of the dsPIC interface, which is a main drawback of the system during implementation stage, the designed controller must adopt a low-order system. Simultaneously, the proposed controller

is expected to provide good performance within the determined weighting constraints. The design procedures for these controllers are provided in this section, ensuring the resolution of the mixed sensitivity problem. This addresses all unpredictable system dynamics such as modeling uncertainties or noises.

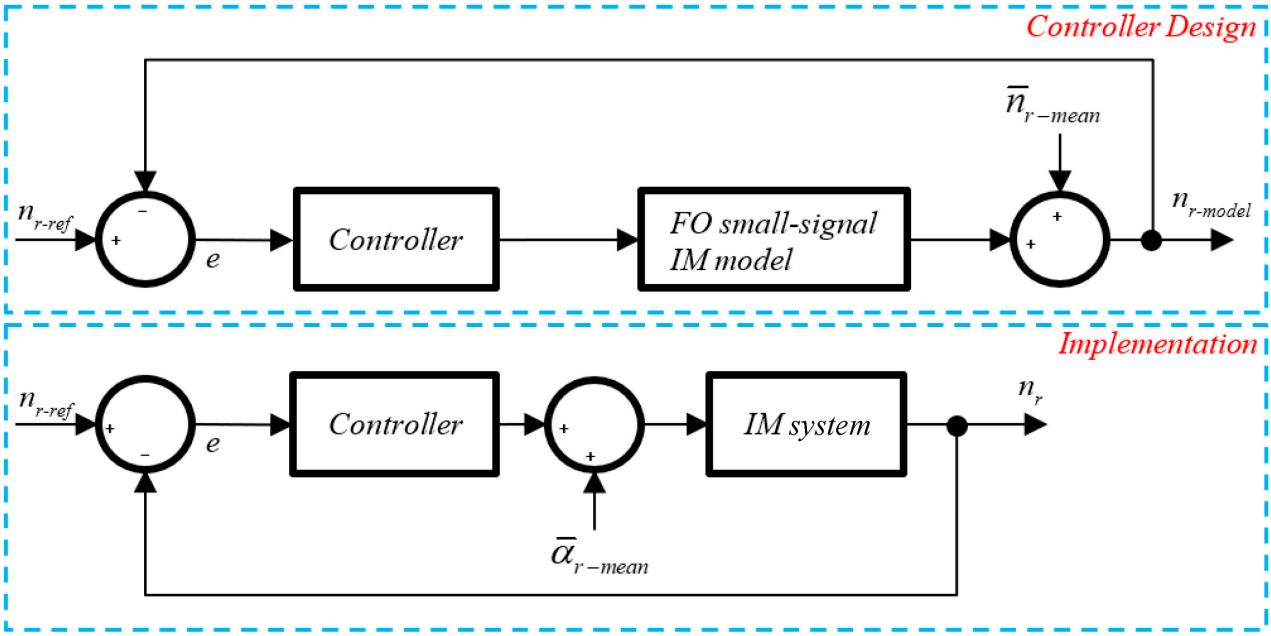


**Figure 7.** The used feedback speed control system for IM.

3.4.1. Robust PID Controller

A classical PID structure is handled as the speed controller to facilitate comparison with the proposed $H_\infty$ controllers. Consequently, by incorporating the specified fractional-order small-signal model into the *pidtool* of the Matlab program, a balance between robustness and nominal performance is achieved. Note that, the step response of the specified fractional-order small-signal model may appear slower than the real-time results. However, achieving the desired trade-off is the primary objective. Based on numerous preliminary experiments, it is deduced that the desired balance between the two frequency-domain requirements should be satisfied in the following manner:

- The suitable bandwidth $\omega_{ol}$ = 0.1676 rad/s;
- The appropriate phase margin $\Delta\phi = 70.2°$.

These requirements are translated into time-domain equivalents, providing a response time of $t_r$ = 8.84 s and a settling time of 35.2 s. The resulting PID speed controller is calculated by the following transfer function.

$$K_{c1} = 1.364e^{-4} + \frac{1.137e^{-4}}{s} - 7.576e^{-4}\frac{s}{5.965s} \tag{16}$$

By applying the designed PID controller to the specified system, a step response is obtained as shown in Figure 8a. Figure 8b,c depict the maximum singular value plots of sensitivity functions for the robust PID controller, illustrating nominal performance and robust stability, respectively.

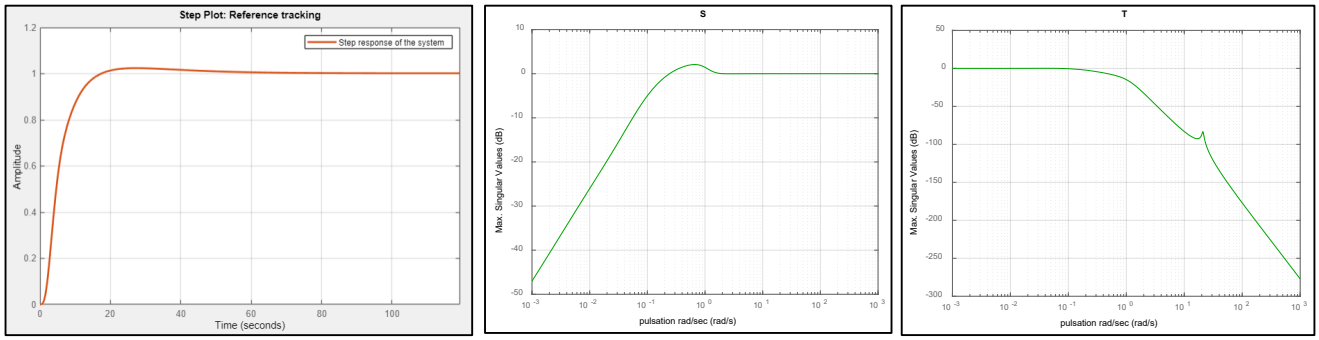


(**a**) Step response of the system (**b**) Nominal performance of PID (**c**) Robust stability of PID

**Figure 8.** Reference tracking performance of designed robust PID controller.

#### 3.4.2. FOPID Based $H_\infty$ Controller

Recent studies have highlighted the superiority of the FOPID controller over the traditional PID controller [2]. The inherent flexibility of the FOPID controller has garnered increased attention from researchers for its application in various industrial systems. Therefore, this study employs a FOPID controller, which is characterized by the transfer function described by the following equation.

$$K_{c2} = K_p + \frac{K_i}{s^{\lambda_c}} + K_d s^{\mu_c} \tag{17}$$

where $K_p, K_i, K_d, \lambda$ and $\mu$ represent the proportional, integral, derivative gains, as well as the order of integrator and derivation, respectively. The parameters of the fractional order weighting function (Equation (15)) and the controller parameters (Equation (17)) must be determined simultaneously to achieve a robust FOPID-based $H_\infty$ controller. Therefore, the design vector, aimed at adjusting the trade-off between robustness and nominal performance, is defined as follows:

$$dp_1 = [\underbrace{K_p, K_i, K_d, \lambda_c, \mu_c}_{FOPID}, \underbrace{M_p, \lambda_1, \omega_{BP}, M_T, \lambda_2, \omega_{BT}}_{dp}] \tag{18}$$

By incorporating the fitness function given in Equation (14) and the specified search space outlined in Equation (15), the design process is transformed into an optimization problem, as presented in Equation (19). This optimization problem can be tackled using the classical PSO algorithm. Employing the small signal method, the average input value ($u$) is subtracted from the measured value, resulting in a highly constrained control signal. Therefore, the constraints on the controller parameters are set to be as minimal as possible. Furthermore, $A_s$ and $A_T$ are held as constants throughout the optimization process, with fixed values of as $5 \times 10^{-2}$ and $1 \times 10^{-3}$, respectively.

$$\begin{aligned} &Min\left\{Max\left(\overline{\sigma}\begin{pmatrix} W_{fs}S \\ W_{ft}T \end{pmatrix}\right)\right\} \\ \text{subject to } dp_1 \begin{cases} (0.01 = M_{P\_\min}) < M_P < (M_{P\_\max} = 3) \\ (0.9 = \lambda_{1\_\min}) < \lambda_1 < (\lambda_{1\_\max} = 1) \\ (0.1 = \omega_{BP\_\min}) < \omega_{BP} < (\omega_{BP\_\max} = 20) \\ (0.01 = M_{T\_\min}) < M_T < (M_{T\_\max} = 3) \\ (0.9 = \lambda_{2\_\min}) < \lambda_2 < (\lambda_{2\_\max} = 1) \\ (0.1 = \omega_{BT\_\min}) < \omega_{BT} < (\omega_{BT\_\max} = 20) \\ (1e^{-7} = K_{p\_\min}) < K_p < (K_{p\_\max} = 1e^{-3}) \\ (1e^{-7} = K_{i\_\min}) < K_i < K_{i\_\max} 1e^{-3}) \\ (-1e^{-6}) = K_{d\_\min} < K_d < (K_{d\_\max} = 1e^{-6}) \\ (0.8 = \lambda_{c\_\min}) < \lambda_c < (\lambda_{c\_\max} = 1) \\ (0.8 = \mu_{c\_\min}) < \mu_c < (\mu_{c\_\max} = 1) \end{cases} \end{aligned} \tag{19}$$

It is evident from Equation (19) that when all the provided guidelines are adhered to, 11 variables will be optimized using the PSO algorithm, with specifications set by the designer. In this paper, to address the challenges associated with complex computations, a high-performance computer is employed for the optimization process. The parameters for configuring the PSO can be found in Table A1 in the Appendix A. It is assumed that the parameters, aside from those in Equation (19), remain constant. Based on preliminary studies and guideline principles, the desired optimal solution for $dp_1$ is determined with regard to the following constraints.

$$\begin{gathered} M_{P\_\min} < (M_P = 2.99) < M_{P\_\max} \\ \lambda_{1\_\min} < (\lambda_1 = 0.90) < \lambda_{1\_\max} \\ \omega_{BP\_\min} < (\omega_{BP} = 0.101) < \omega_{BP\_\max} \\ M_{T\_\min} < (M_T = 2.97) < M_{T\_\max} \\ \lambda_{2\_\min} < (\lambda_2 = 0.99) < \lambda_{2\_\max} \\ \omega_{BT\_\min} < (\omega_{BT} = 17.22) < \omega_{BT\_\max} \\ K_{p\_\min} < (K_p = 1.73\mathrm{e}^{-4}) < K_{p\_\max} \\ K_{i\_\min} < (K_i = 1.59\mathrm{e}^{-4}) < K_{i\_\max} \\ K_{d\_\min} < (K_d = 9.49\mathrm{e}^{-5}) < K_{d\_\max} \\ \lambda_{c\_\min} < (\lambda_c = 0.9815) < \lambda_{c\_\max} \\ \mu_{c\_\min} < (\mu_c = 0.8181) < \mu_{c\_\max} \end{gathered} \tag{20}$$

where the frequency range is considered as $\omega_r \in [10^{-4}, 10^3]$ rad/s. The optimization process concludes with $\gamma$ = 0.523, representing the optimal minimization result. As a result, a satisfactory performance level that fulfills the conditions for weighted mixed sensitivity within the specified frequency range is achieved. The optimization results yield the following weighting functions.

$$\begin{gathered} W_s = \frac{(\mathrm{s}^{0.9039}+0.101)/(2.99)}{\mathrm{s}^{0.9039}+(5\mathrm{e}^{-2}\cdot 0.101)} \\ W_T = \frac{(\mathrm{s}^{0.99}/17.22)+(1/2.97)}{1+\mathrm{s}^{0.99}(1\mathrm{e}^{-3}/17.220)} \\ where \begin{cases} M_{P\_\min} < M_P < M_{P\_\max} \\ \lambda_{1\_\min} < \lambda_1 < \lambda_{1\_\max} \\ \omega_{BP\_\min} < \omega_{BP} < \omega_{BP\_\max} \\ M_{T\_\min} < M_T < M_{T\_\max} \\ \lambda_{2\_\min} < \lambda_2 < \lambda_{2\_\max} \\ \omega_{BT\_\min} < \omega_{BT} < \omega_{BT\_\max} \end{cases} \end{gathered} \tag{21}$$

Equation (21) demonstrates that the optimized parameters fall within the specified limits. The fractional-order weighting functions are obtained in this manner. In addition to the weighting functions, the optimization process yields the optimal parameters of the robust FOPID controller, as shown in Equation (22). The main advantage of the proposed method is that it allows for the simultaneous determination of weighting functions, and controller parameters are conducted regardless of violating the guideline rules. Thus, a trade-off between nominal performance and robustness is guaranteed.

$$K_{c2} = 1.73\mathrm{e}^{-4} + \frac{1.59\mathrm{e}^{-4}}{s^{0.9815}} + 9.49\mathrm{e}^{-5}s^{0.8181} \tag{22}$$

Referring to Equations (21) and (22), a frequency domain analysis is conducted. It is evident from Figure 9 that maximum singular value (in dB) plots show that the $\overline{\sigma}({W_S}^{-1})$ curve exhibits a smooth response at low frequencies ($\omega_r < 10^{-2}$), while the $\overline{\sigma}({W_T}^{-1})$ curve remains flat at high frequencies ($\omega_r > 10^1$). These curves suggest that the obtained ${W_S}^{-1}$ provides excellent tracking dynamics at low frequencies, while the achieved ${W_T}^{-1}$ enhances robustness against noise and uncertainties at high frequencies. Furthermore, the maximum singular value plots of sensitivity functions derived from the FOPID controller lie below

the specified weighting functions. As shown in Figure 9, the robust FOPID controller is effectively synthesized without violating the constraints of ${W_S}^{-1}$ and ${W_T}^{-1}$. The maximum singular values plot for S-T comparison is depicted in Figure 10. This plot illustrates that the trade-off between sensitivity functions remains below $-5.5$, confirming that the safety margin, ensuring the identity function $S + T = I$, has been achieved [35].

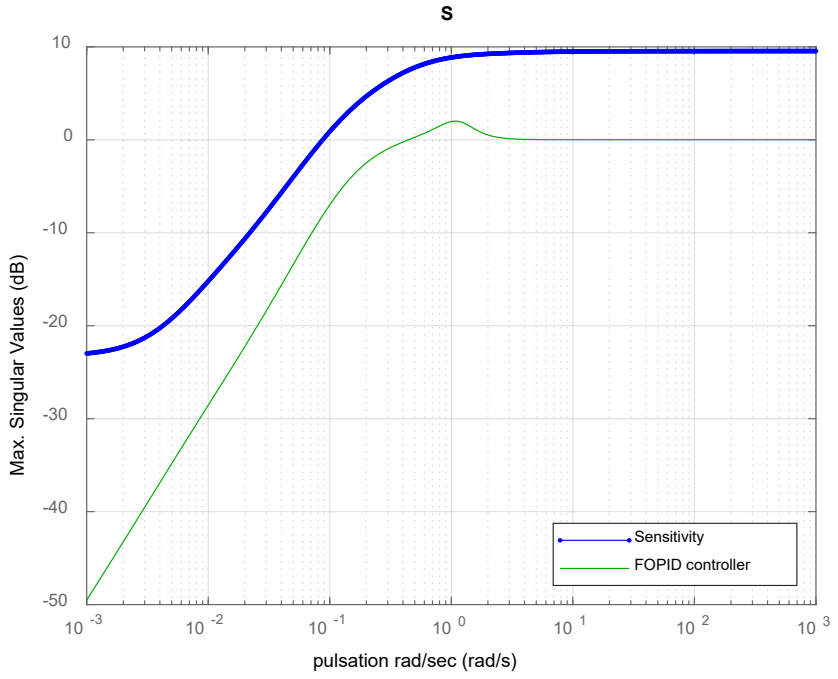


(**a**)

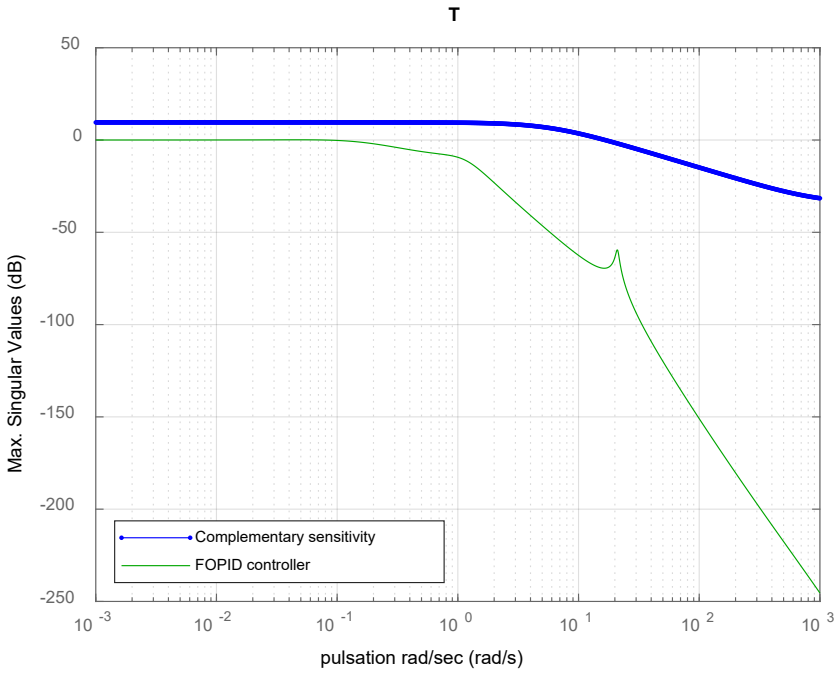


(**b**)

**Figure 9.** Maximal singular value plots of the sensitivity functions with FOPID controller. (**a**) Sensitivity of FOPID controller, (**b**) Complementary sensitivity of FOPID controller.

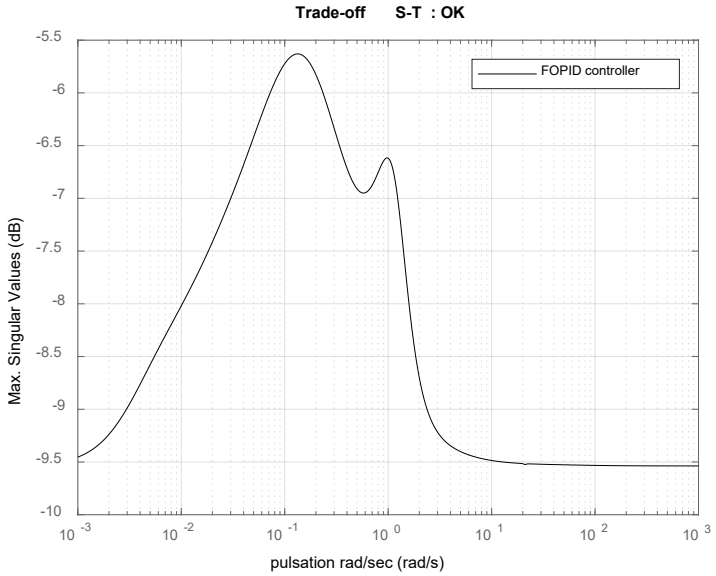


**Figure 10.** Trade-off between S-T.

3.4.3. Fixed-Structure $H_\infty$ Controller

In this section, a fixed structure $H_\infty$ controller that ensures nominal performance and robust stability is designed using the previously obtained optimal weighting functions. The 'hinfstruct' command within the Matlab program is employed to synthesize the proposed controller. This command tunes the parametric control block '*K*' depicted in Figure 5. The tuning process aims to minimize the $H_\infty$ norm of the closed loop transfer function, which includes fractional order small-signal model (Equation (6)). While 'hinfsyn' can provide a smaller $H_\infty$ norm, it results in high-order controllers that are not suitable for microcontrollers. Therefore, this study defines the boundaries of the robust controller using 'hinfstruct'.

The configuration options for the optimization algorithm in 'hinfstruct' are as follows:

1. 'Targetgain = 0′ stops the optimization once the target $H_\infty$ is achieved.
2. 'Randomstart = 10′ prevents local minima.
3. 'Display final' indicates the optimization results at each iteration.
4. 'tunableSS ('$H_{str}$',5,1,1)' selects controller '$H_{str}$' with a single input-single output.
5. Construction of sensitivity functions.
6. 'blkdiag' forms a block diagonal matrix from production of weighting functions and sensitivity functions.
7. 'hinfstruct' tunes the controller.

After successful optimization, $H_\infty$ of the designed controller is calculated to be 0.4847. Additionally, the state-space model data of the designed controller are provided below:

$$
\begin{aligned}
A_{H_{str}} &= \begin{bmatrix} -8.30 & 40.20 & 0 & 0 & 0 \\ -3.71 & -8.16 & -0.61 & 0 & 0 \\ 0 & 11.72 & 0.99 & 1.58 & 0 \\ 0 & 0 & -21.75 & -46.59 & 10.85 \\ 0 & 0 & 0 & -3.29 & -36.53 \end{bmatrix} \\
B_{H_{str}} &= \begin{bmatrix} -2.82 \\ -0.18 \\ -0.61 \\ 0.55 \\ 1.45 \end{bmatrix} \\
C_{H_{str}} &= [0.07 -0.61\ 0.79\ 1.76\ 0.03] \\
D_{H_{str}} &= \left[7.45\mathrm{e}^{-04}\right]
\end{aligned}
\tag{23}
$$

The frequency analysis of the closed-loop control system with the $H_{str}$ controller can be conducted using Bode diagrams, as shown in Figure 11. It is evident from the Bode plots that both responses meet the requirements defined by the fractional order weighting functions. Therefore, it can be concluded that the designed $H_{str}$ controller guarantees nominal performance and robust stability. However, a better nominal performance is achieved when the maximum singular values are minimized in the sensitivity matrix at low frequencies. Conversely, superior robust stability is ensured when the maximum singular values are minimized in the complementary sensitivity matrix at low frequencies [22].

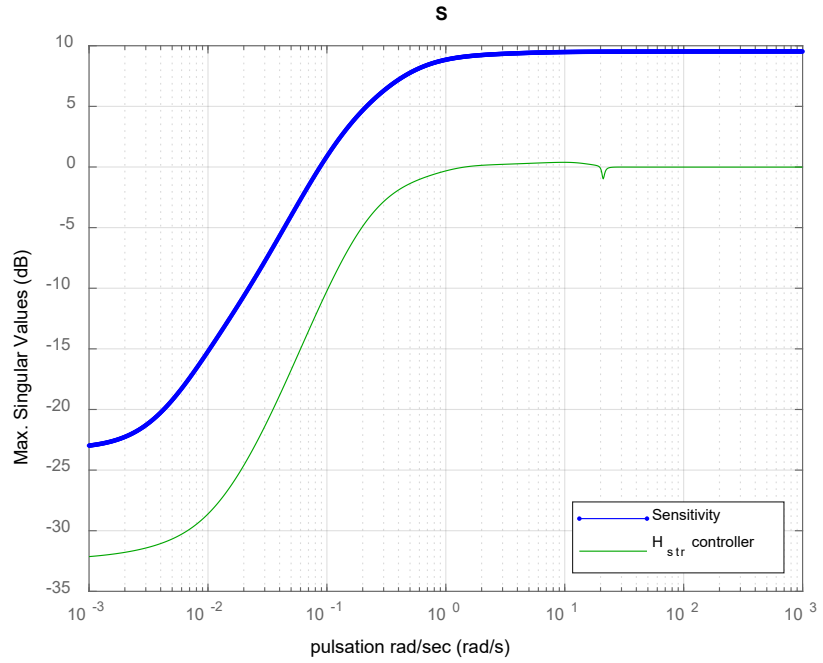


(**a**)

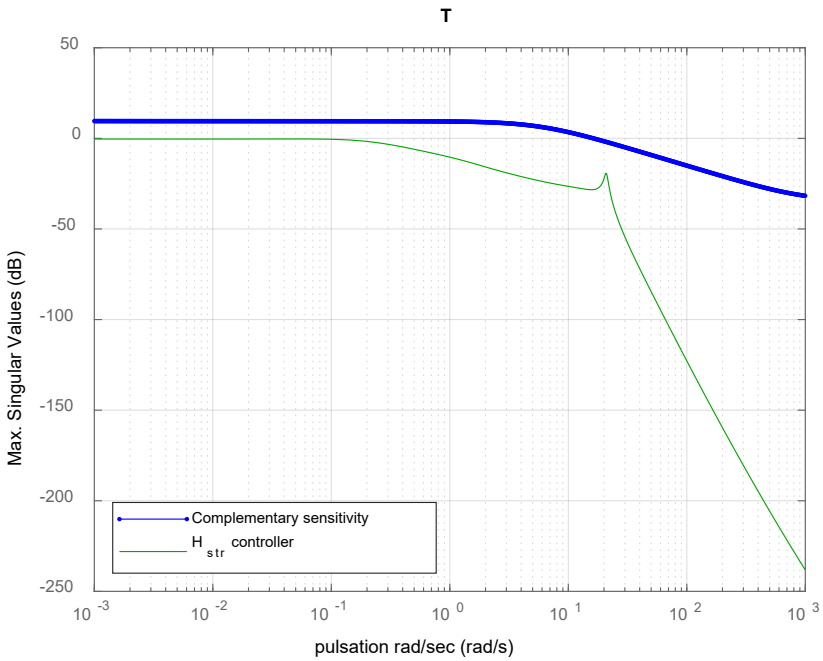


(**b**)

**Figure 11.** Max. singular values plots of the sensitivity functions with $H_{str}$ controller. (**a**) Sensitivity of $H_{str}$ controller, (**b**) Complementary sensitivity of $H_{str}$ controller.

It is evident from Figures 8, 9 and 11 that the FOPID controller provides a better nominal performance margin. It exhibits the smallest maximum singular value in the direct sensitivity function. Furthermore, in the low-frequency range, below $10^{-2}$ rad/s, the maximum singular value curve of the direct sensitivity function remains at nearly $-20$ dB. This demonstrates that load disturbances are attenuated by more than 31.62 times at the plant output. Conversely, the robust PID controller offers a superior robust stability margin. The maximum singular value plots of the complementary sensitivity function reveal that PID has the smallest value at $10^{-3}$ rad/s. Additionally, beyond $10^{2}$ rad/s, the curve drops below $-150$ dB, indicating that sensor noise suppression exceeds 1e$^{6}$ times at the plant output.

## 4. Results and Discussion

To assess and compare the effectiveness of the designed controllers in terms of robustness and noise suppression, the experimental setup outlined in the relevant section is employed. The feedback control system is subjected to various reference input vectors. Additionally, the system experiences disturbances as an input vector which consist of an additional load (30% of the nominal power) applied at the starting time, around t = 60 s. This disturbance is removed at t = 60 s once the system reaches the desired reference. After t = 120 s, artificial sensor noise is introduced to speed measurement. The noise takes the form of a uniform random number between $\pm$25 rpm. Due to the fractional-order small signal model and structure of the experimental setup, the speed is expressed in actual speed in rpm, while the triggering command is presented as PWM%. As a result, in the experimental results, control signals are represented between 0–1 PWM%.

Clearly observed from Figures 12–14, the designed robust controllers successfully ensure reference tracking. Each of them exhibits a smooth speed response with minimal rise and settling times. Figure 12 shows that the robust PID controller achieves a settling time of 8 s without any overshoot. It effectively guides the system trajectories toward the selected references, demonstrating robustness against both load disturbances and sensor noises. Whenever a load disturbance is introduced or removed from the system, the robust PID controller effectively rejects the disturbance and quickly reaches the reference. Moreover, after t = 120 s, when subjected to noise, the closed-loop robustness is also well maintained. The robust PID controller remains largely unaffected by measurement noise, as evident from its control signal in Figure 12.

Figure 13 illustrates that the fixed-structure $H_\infty$ controller achieves a settling time of 8 s without any overshoot. Its capacity to track various references while maintaining closed-loop robustness against load disturbances is evident. When load disturbances are introduced or removed from the system, it tracks the reference promptly while rejecting the disturbance. However, it shows sensitivity to sensor noises, affecting the speed response. Additionally, the control signal displays chattering effects, which persist whether artificial noise is present or not. This situation raises a concern: the microcontroller of the system (dsPIC) may not meet the memory requirements of the designed fixed-structure $H_\infty$ controller. A potential solution to the chattering problem might involve using a more suitable microcontroller in place of the dsPIC.

Finally, the $H_\infty$-based FOPID controller outperforms the other designed controllers in terms of tracking dynamics. Neither load disturbances nor sensor noises manage to compromise the robustness of the FOPID controller. Right from the start, it efficiently tracks various references, achieving a short settling time of 6 s without any overshoot. As depicted in Figure 14, whenever there is a change in the reference, the FOPID controller consistently responds more quickly compared to the others and reaches the new reference. Furthermore, in the presence of an external load, it rapidly rejects the disturbance within 5 s, and brings the trajectories to equilibrium. Importantly, sensor noises do not significantly disrupt its performance.

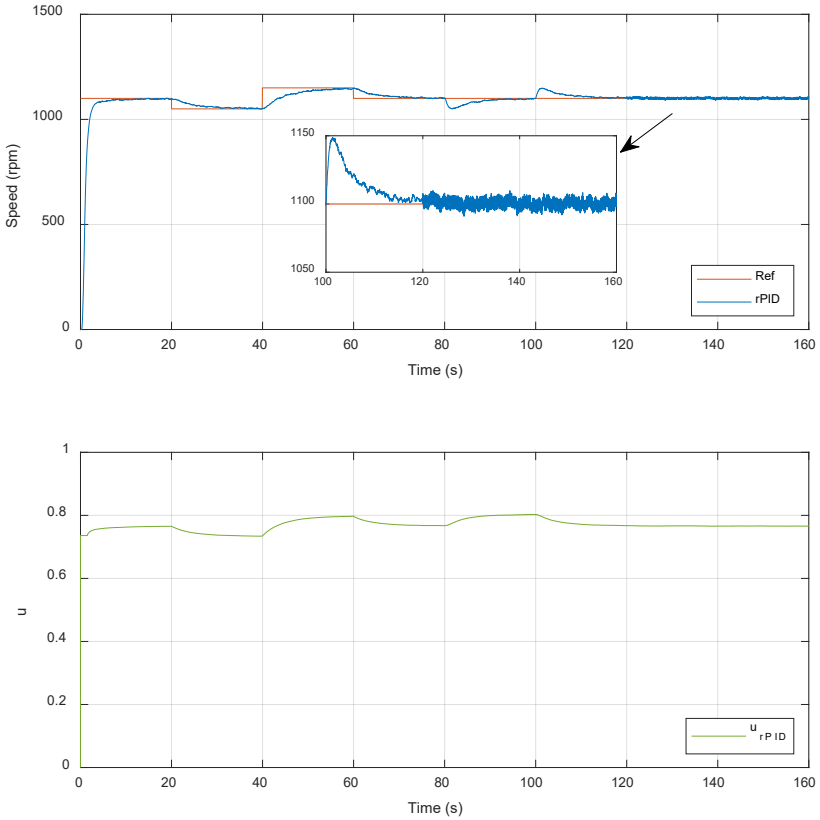


**Figure 12.** Speed control of the IM by employing robust PID (rPID), process output (y) and relevant control signal (u).

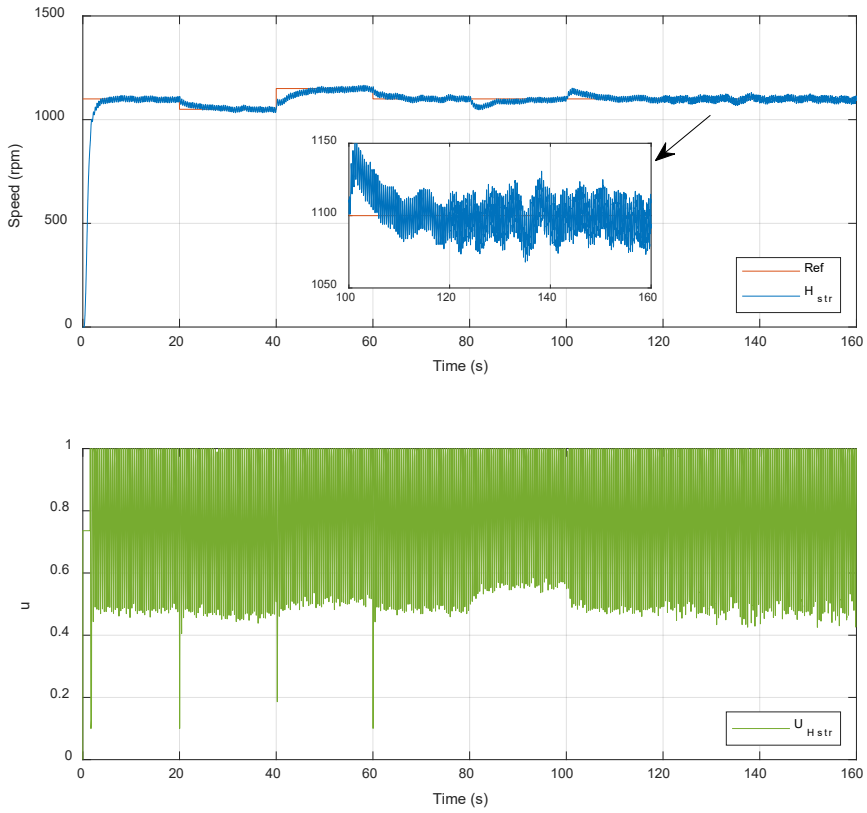


**Figure 13.** Speed control of the IM by employing fixed-structure $H_\infty$ controller, process output (y) and relevant control signal (u).

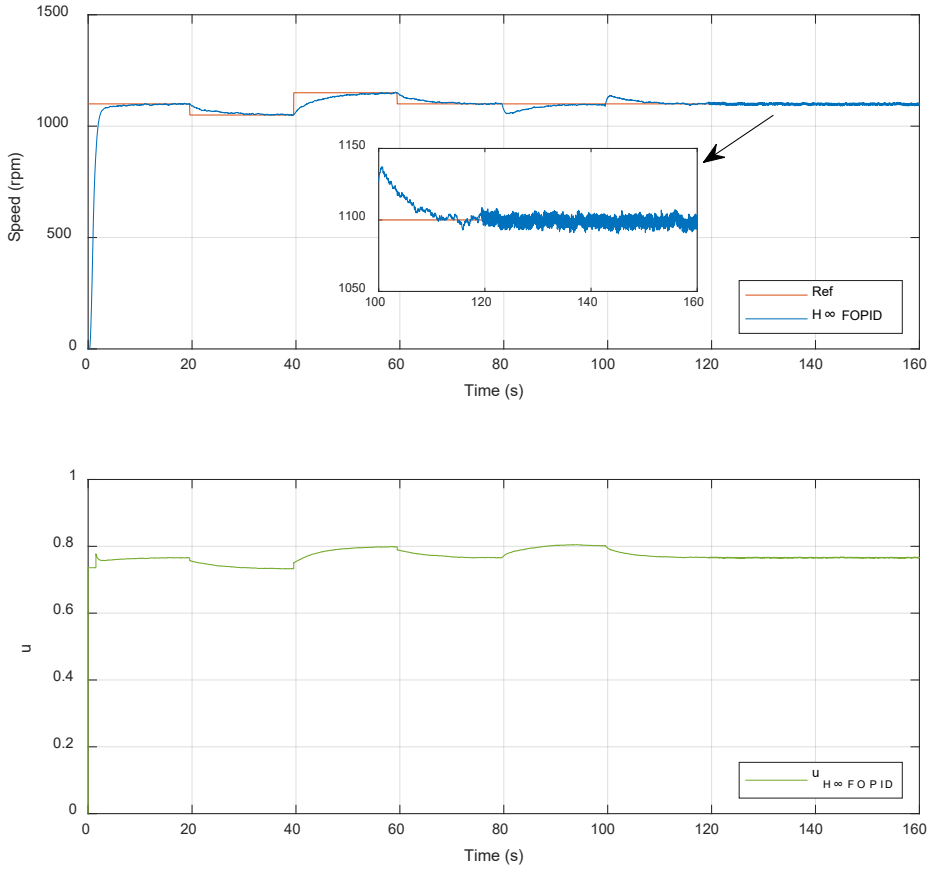


**Figure 14.** Speed control of the IM by employing $H_\infty$-based FOPID controller, process output (y) and relevant control signal (u).

## 5. Conclusions

This paper introduces a robust speed controller for the IM, specifically addressing the solution of the $H_\infty$ weighted mixed sensitivity problem. However, the uncertainty in the knowledge of machine model and the selection of weighting functions remain major challenges for the proposed method. To address these challenges, the paper begins with fractional order small signal modeling. This entails using the triggering command (PWM duty cycle) as the input and the motor's angular speed as the output. It has been demonstrated that when compared to integer order modeling, this designed model effectively estimates speed with a high accuracy rate (95%). Subsequently, robust speed controllers are synthesized based on the mixed sensitivity problem using fractional order weighting matrices. Three robust speed controllers are developed using Matlab's *pidtool* function, structured $H_\infty$, and $H_\infty$-based FOPID controller. The appropriate bandwidth and phase margin are chosen as 0.1676 rad/s and 70.2°, respectively, in *pidtool*. The $H_\infty$ norms of structured $H_\infty$ and $H_\infty$-based FOPID controllers are determined to be 0.4847 and 0.523. Frequency responses of these designed controllers are analyzed using Bode diagrams to determine whether they violate the specified robustness and nominal performance limits. After confirming the robustness and strong tracking performance of the controllers, real-time implementations are conducted. All controllers not only exhibit effective tracking dynamics but also robustness against load disturbances, thereby validating the capability of the designed fractional-order small-signal model. Among the designed controllers, the $H_\infty$-based FOPID demonstrates the best tracking dynamics with a 6 s settling time and no overshoot. The FOPID controller effectively rejects load variations and suppresses sensor noises. On the other hand, the PID controller exhibits behavior similar to the FOPID controller but with a slightly longer settling time of 8 s, showing some deficiencies in tracking performance. Finally, the fixed-structure $H_\infty$ controller excels in tracking the

reference with an 8-s settling time, but falls short in handling sensor noises. It is evident that the fixed structure lacks the flexibility required for effective noise suppression. Therefore, future work may involve the design of a fixed-structure fractional-order $H_\infty$ speed controller for IM.

**Funding:** This research received no external funding.

**Data Availability Statement:** Not applicable.

**Conflicts of Interest:** The author declares no conflict of interest.

## Appendix A

**Table A1.** PSO configuration parameters.

| Parameter | Value |
|---|---|
| CreationFcn | @pswcreationuniform |
| Display | 'final' |
| FunctionTolerance | $1.0000 \times 10^6$ |
| HybridFcn | [] |
| InertiaRange | [0.1000,1.1000] |
| InitialSwarmMatrix | [] |
| InitialSwarmSpan | 2000 |
| MaxIterations | '200*numberofvariables' |
| MaxStallIterations | 20 |
| MaxStallTime | Inf |
| MaxTime | Inf |
| MinNeighborsFraction | 0.2500 |
| ObjectiveLimit | -Inf |
| OutputFcn | [] |
| PlotFcn | @pswplotbestf |
| SelfAdjustmentWeight | 1.4900 |
| SocialAdjustmentWeight | 1.4900 |
| SwarmSize | 'min(100,10*numberofvariables)' |
| UseParallel | 0 |
| UseVectorized | 0 |

## References

1. Ilten, E. Conformable Fractional Order Controller Design and Implementation for Per-Phase Voltage Regulation of Three-Phase SEIG Under Unbalanced Load. *Electr. Power Compon. Syst.* **2022**, *50*, 636–648. [CrossRef]
2. Demirtas, M.; Ilten, E.; Calgan, H. Pareto-Based Multi-objective Optimization for Fractional Order PIλ Speed Control of Induction Motor by Using Elman Neural Network. *Arab. J. Sci. Eng.* **2019**, *44*, 2165–2175. [CrossRef]
3. Talla, J.; Leu, V.Q.; Šmídl, V.; Peroutka, Z. Adaptive speed control of induction motor drive with inaccurate model. *IEEE Trans. Ind. Electron.* **2018**, *65*, 8532–8542. [CrossRef]
4. Sung, W.; Shin, J.; Jeong, Y. Energy-efficient and robust control for high-performance induction motor drive with an application in electric vehicles. *IEEE Trans. Veh. Technol.* **2012**, *61*, 3394–3405. [CrossRef]
5. Lin, F.-J.; Wai, R.-J. Robust control using neural network uncertainty observer for linear induction motor servo drive. *IEEE Trans. Power Electron.* **2002**, *17*, 241–254.
6. Alonge, F.; Cirrincione, M.; D'Ippolito, F.; Pucci, M.; Sferlazza, A. Robust active disturbance rejection control of induction motor systems based on additional sliding-mode component. *IEEE Trans. Ind. Electron.* **2017**, *64*, 5608–5621. [CrossRef]
7. Pohl, L.; Vesely, I. Speed control of induction motor using H∞ linear parameter varying controller. *IFAC-PapersOnLine* **2016**, *49*, 74–79. [CrossRef]
8. Qu, H.; Zhao, J. Event-triggered H∞ control for switched interval type-2 fuzzy systems under denial-of-service. *Int. J. Robust Nonlinear Control* **2023**, *33*, 2219–2237. [CrossRef]
9. Ilten, E.; Calgan, H.; Demirtas, M. Design of induction motor speed observer based on long short-term memory. *Neural Comput. Appl.* **2022**, *34*, 18703–18723. [CrossRef]

10. Acevedo, S.S.; Giraldo, E.; Giraldo, D. Speed control of induction motor using robust control with lsdp. In Proceedings of the Electronics, Robotics and Automotive Mechanics Conference, Online, 30 September–3 October 2008; IEEE: New York, NY, USA, 2008; pp. 350–353.
11. Mohamed, A. Modern robust control of a CSI-fed induction motor drive system. In Proceedings of the 1998 American Control Conference ACC, Philadelphia, PA, USA, 24–26 June 1998; (IEEE Cat. No. 98CH36207); IEEE: New York, NY, USA, 1998; Volume 6, pp. 3803–3808.
12. Allag, M.; Allag, A.; Zeghib, O.; Hamidani, B. Robust h∞ control based on the mean value theorem for induction motor drive. *J. Control Autom. Electr. Syst.* **2019**, *30*, 657–665. [CrossRef]
13. Kaitwanidvilai, S.; Olranthichachart, P.; Ngamroo, I. PSO based automatic weight selection and fixed structure robust loop shaping control for power system control applications. *Int. J. Innov. Comput. Inf. Control* **2011**, *7*, 1549–1563.
14. Kaur, R.; Ohri, J. PSO based weight selection and fixed structure robust loop shaping control for pneumatic servo system with 2DOF controller. *Int. J. Electr. Comput. Eng.* **2015**, *8*, 1365–1373.
15. Amieur, T.; Bechouat, M.; Sedraoui, M.; Kahla, S.; Guessoum, H. A new robust tilt-PID controller based upon an automatic selection of adjustable fractional weights for permanent magnet synchronous motor drive control. *Electr. Eng.* **2021**, *103*, 1881–1898. [CrossRef]
16. Avci, D.; Ozdemir, N.; Yavuz, M. *Fractional Optimal Control of Diffusive Transport Acting on a Spherical Region*; CRC Press: Boca Raton, FL, USA, 2019; Volume 1.
17. Daraz, A.; Malik, S.A.; Basit, A.; Aslam, S.; Zhang, G. Modified FOPID controller for frequency regulation of a hybrid interconnected system of conventional and renewable energy sources. *Fractal Fract.* **2023**, *7*, 89. [CrossRef]
18. El-Sousy, F.F.M.; Alqahtani, M.H.; Aljumah, A.S.; Aly, M.; Almutairi, S.Z.; Mohamed, E.A. Design Optimization of Improved Fractional-Order Cascaded Frequency Controllers for Electric Vehicles and Electrical Power Grids Utilizing Renewable Energy Sources. *Fractal Fract.* **2023**, *7*, 603. [CrossRef]
19. Zaid, S.A.; Bakeer, A.; Magdy, G.; Albalawi, H.; Kassem, A.M.; El-Shimy, M.E.; AbdelMeguid, H.; Manqarah, B. A new intelligent fractional-order load frequency control for interconnected modern power systems with virtual inertia control. *Fractal Fract.* **2023**, *7*, 62. [CrossRef]
20. Makhbouche, A.; Boudjehem, B.; Birs, I.; Muresan, C.I. Fractional-order PID controller based on immune feedback mechanism for time-delay systems. *Fractal Fract.* **2023**, *7*, 53. [CrossRef]
21. Rahman, M.Z.U.; Leiva, V.; Martin-Barreiro, C.; Mahmood, I.; Usman, M.; Rizwan, M. Fractional transformation-based intelligent H-infinity controller of a direct current servo motor. *Fractal Fract.* **2022**, *7*, 29. [CrossRef]
22. Sedraoui, M.; Amieur, T.; Bachir Bouiadjra, R.; Sahnoune, M. Robustified fractional-order controller based on adjustable fractional weights for a doubly fed induction generator. *Trans. Inst. Meas. Control* **2017**, *39*, 660–674. [CrossRef]
23. Amieur, T.; Younsi, A.; Aidoud, M.; Sedraoui, M.; Amieur, O. Design of robust fractional order PID controller using fractional weights in the mixed sensitivity problem. In Proceedings of the 2017 14th International Multi-Conference on Systems, Signals & Devices, Marrakech, Morocco, 28–31 March 2017; IEEE: New York, NY, USA, 2017; pp. 549–553.
24. Menak, R.; Tan, N. Design of Robust Integer/Fractional Order PID Controller Based on Bode's Ideal Transfer Function and H-Infinity Robust Performance Condition. In Proceedings of the 2023 International Conference on Fractional Differentiation and Its Applications, Ajman, United Arab Emirates, 14–16 March 2023; IEEE: New York, NY, USA, 2023; pp. 1–6.
25. Yaghi, M.; Efe, M.Ö. H2/H∞-Neural-Based FOPID Controller Applied for Radar-Guided Missile. *IEEE Trans. Ind. Electron.* **2019**, *67*, 4806–4814. [CrossRef]
26. Zamani, M.; Karimi-Ghartemani, M.; Sadati, N. FOPID controller design for robust performance using particle swarm optimization. *Fract. Calc. Appl. Anal.* **2007**, *10*, 169–187.
27. Demirtas, M.; Calgan, H.; Toufik, A.; Sedraoui, M. Small-signal modeling and robust multi-loop PID and H∞ controllers synthesis for a self-excited induction generator. *ISA Trans.* **2021**, *117*, 234–250. [CrossRef] [PubMed]
28. Tepljakov, A. Fractional-Order Calculus Based Identification and Control of Linear Dynamic Systems. Master's Thesis, Tallinn University of Technology, Tallinn, Estonia, 2011.
29. Yan, Z.; Utkin, V. Sliding mode observers for electric machines-an overview. In Proceedings of the IEEE 2002 28th Annual Conference of the Industrial Electronics Society, IECON 02, Sevilla, Spain, 5–8 November 2002; IEEE: New York, NY, USA, 2002; Volume 3, pp. 1842–1847.
30. Ilten, E. Conformable fractional order controller design and optimization for sensorless control of induction motor. *COMPEL- Int. J. Comput. Math. Electr. Electron. Eng.* **2022**, *41*, 1528–1541. [CrossRef]
31. Dey, N.; Mondal, U.; Mondal, D. Design of a H-infinity robust controller for a DC servo motor system. In Proceedings of the 2016 International Conference on Intelligent Control Power and Instrumentation, Kolkata, India, 21–23 October 2016; IEEE: New York, NY, USA, 2016; pp. 27–31.
32. Ortega, M.G.; Rubio, F.R. Systematic design of weighting matrices for the H∞ mixed sensitivity problem. *J. Process Control* **2004**, *14*, 89–98. [CrossRef]

33. Papalambrou, G.; Karlis, E.; Kyrtatos, N. Robust control of manifold air injection in a marine diesel engine. *IFAC-PapersOnLine* **2015**, *48*, 438–443. [CrossRef]
34. Oloomi, H.; Shafai, B. Weight selection in mixed sensitivity robust control for improving the sinusoidal tracking performance. In Proceedings of the 42nd IEEE International Conference on Decision and Control, MAUI, HI, USA, 9–12 December 2003; (IEEE Cat. No. 03CH37475); IEEE: New York, NY, USA, 2003; Volume 1, pp. 300–305.
35. Rao, S.S. *Engineering Optimization: Theory and Practice*; John Wiley & Sons: Hoboken, NJ, USA, 2019.